

Análise Microestrutural usando a Difração de Raio-X e o Método de Rietveld

Prof. Dr. Haroldo Cavalcanti Pinto

haroldo@sc.usp.br

2º Semestre de 2016

Um cristal é geralmente definido como *um sólido com seus átomos arranjados em um reticulado periódico tridimensional.*

Idealmente, o arranjo mais estável dos átomos em um cristal será aquele que minimiza a energia livre por unidade de volume ou, em outras palavras, aquele que:

- preserva a neutralidade elétrica;
- satisfaz o caráter direcional das ligações covalentes;
- minimiza as repulsões íon-íon e, além disto,
- agrupa os átomos o mais compactamente possível.

A grande maioria dos sólidos é cristalina. Os cristais encontrados na natureza tiveram um crescimento muito lento ao longo dos processos geológicos e são geralmente muito maiores que os produzidos sinteticamente.

Mas nem todos os sólidos são cristalinos. Alguns, como os vidros e as resinas termorígidas são totalmente amorfos. Outros, como muitos termoplásticos apresentam regiões cristalinas em uma matriz amorfa.

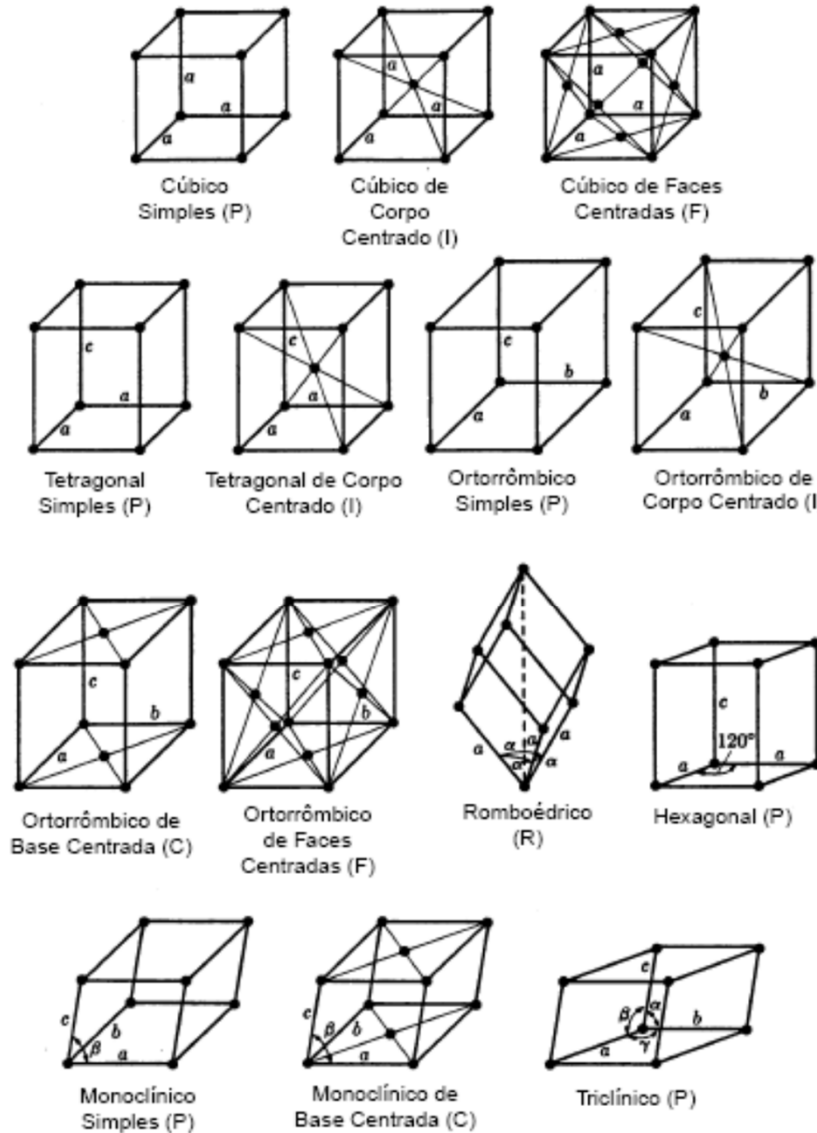


Figura 4.2 — Os 14 reticulados de Bravais.

Tabela 4.1 — Parâmetros de rede e ângulos dos 7 sistemas de Bravais

Sistema	Parâmetros de rede	Ângulos
cúbico	$a = b = c$	$\alpha = \beta = \gamma = 90^\circ$
tetragonal	$a = b \neq c$	$\alpha = \beta = \gamma = 90^\circ$
ortorrômico	$a \neq b \neq c$	$\alpha = \beta = \gamma = 90^\circ$
romboédrico	$a = b = c$	$\alpha \neq \beta \neq \gamma \neq 90^\circ$
hexagonal	$a = b \neq c$	$\alpha = \beta = 90^\circ; \gamma = 120^\circ$
monoclínico	$a \neq b \neq c$	$\alpha = \gamma = 90^\circ; \beta > 90^\circ$
triclinico	$a \neq b \neq c$	$\alpha \neq \beta \neq \gamma \neq 90^\circ$

Como existem muitas estruturas cristalinas possíveis, é conveniente dividí-las em grupos de acordo com as configurações da célula unitária e/ou arranjos atômicos. Tal esquema baseia-se na geometria da célula unitária, isto é, a forma do paralelepípedo (célula) unitário(a) apropriado(a) sem levar em conta as posições atômicas na célula. Um sistema de coordenadas x , y e z é estabelecido com a sua origem em um dos cantos da célula unitária; cada um dos eixos x , y e z coincide com uma das 3 arestas do paralelepípedo que se estendem a partir deste canto, como ilustrado na Figura. A geometria da célula unitária é completamente definida em termos de 6 parâmetros: os 3 comprimentos de arestas a , b e c , e os 3 ângulos α , β e γ . Estes estão indicados na Figura e são às vezes denominados parâmetros de rede de uma estrutura cristalina.

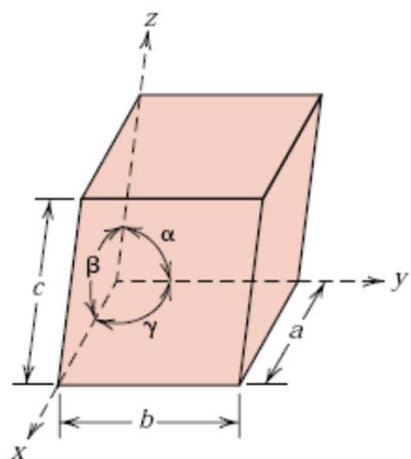
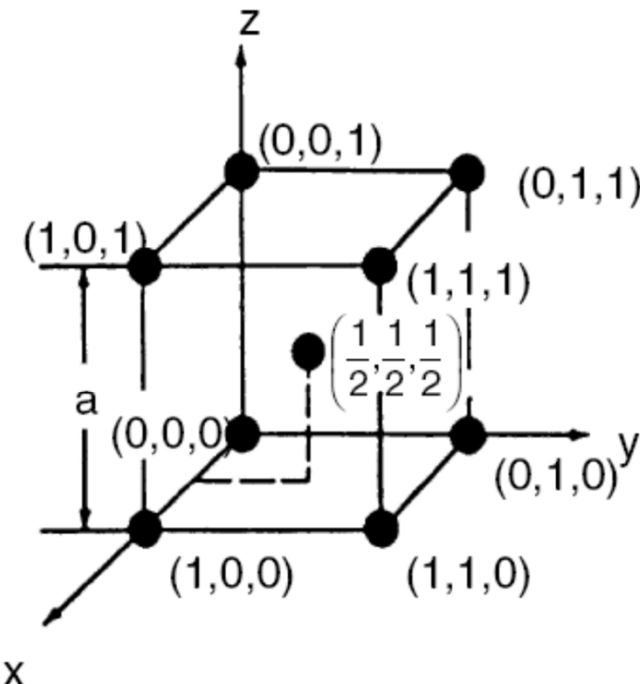
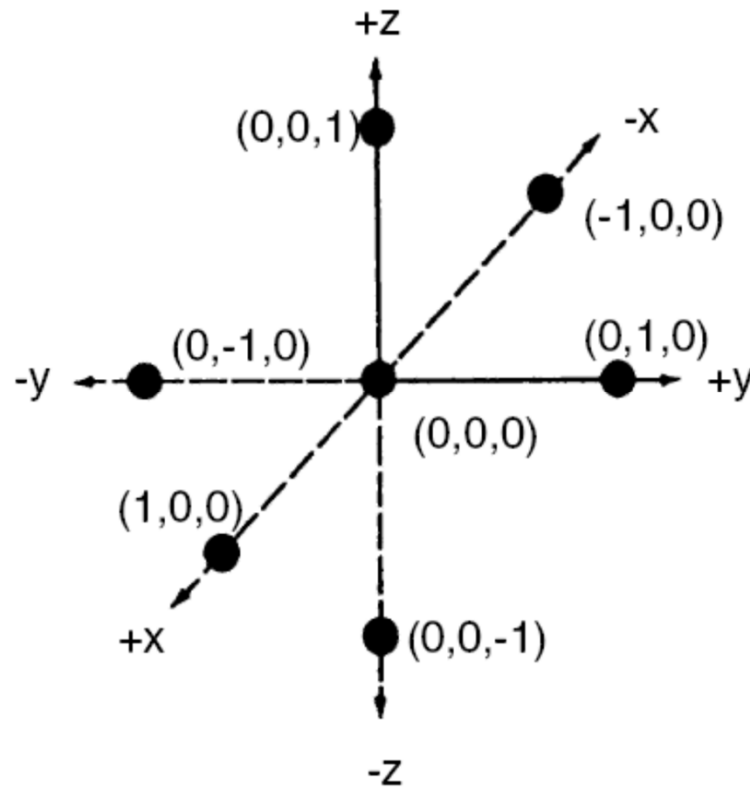


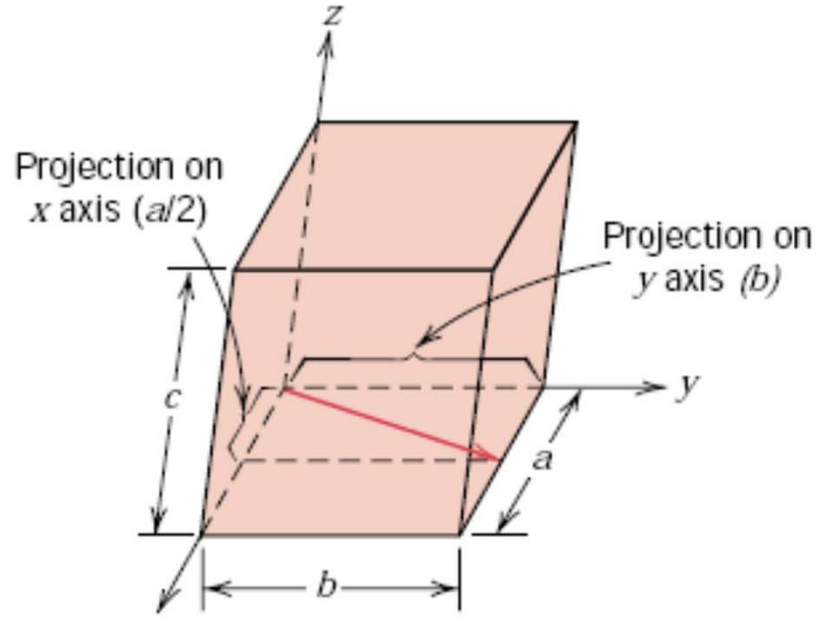
FIGURE 3.19 A unit cell with x , y , and z coordinate axes, showing axial lengths (a , b , and c) and interaxial angles (α , β , and γ).



As posições dos átomos são definidas com respeito à origem do sistema de coordenadas compatível com a geometria do cristal

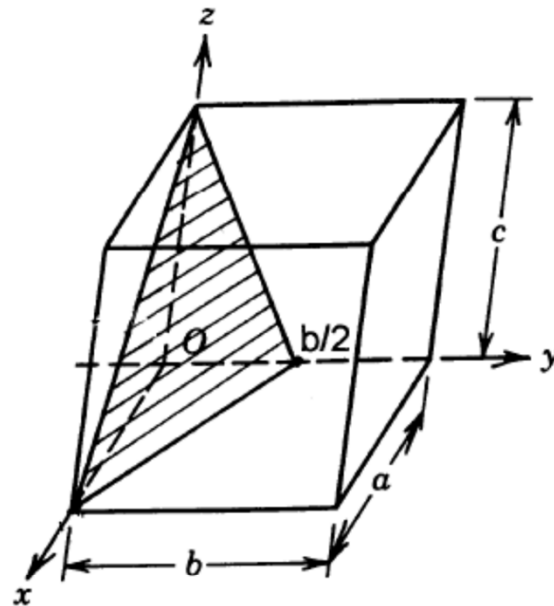
Os parâmetros de rede nas direções dos eixos x, y e z representam a unidade do sistema de posicionamento dos átomos

Átomos localizados dentro da célula unitária apresentam coordenadas sempre menor que 1, como por ex.: $(\frac{1}{2}, \frac{1}{2}, \frac{1}{2})$



	x	y	z
Projeção	$a/2$	b	$0c$
Projeção em termos de a, b, c	$1/2$	1	0
Redução a mínimos inteiros	1	2	0
Notação	[120]		

Figura 5.1 — Exemplo de indexação de uma direção cristalográfica no sistema proposto por Miller.



	x	y	z
Interceptos	a	$b/2$	c
Interceptos em termos de a, b, c	1	$1/2$	1
Recíprocos	1	2	1
Recíprocos reduzidos	1	2	1
Notação	(121)		

Figura 5.2 — Exemplo de indexação de um plano cristalográfico no sistema proposto por Miller.

Tabela 5.1 — Relações entre o espaçamento interplanar (d), os parâmetros de reticulado (a, b, c), os ângulos entre planos (α, β, γ) e os planos ($h k l$).

Cúbico:
$$\frac{1}{d^2} = \frac{h^2 + k^2 + l^2}{a^2}$$

Tetragonal:
$$\frac{1}{d^2} = \frac{h^2 + k^2}{a^2} + \frac{l^2}{c^2}$$

Hexagonal:
$$\frac{1}{d^2} = \frac{4}{3} \left(\frac{h^2 + hk + k^2}{a^2} \right) + \frac{l^2}{c^2}$$

Romboédrico:
$$\frac{1}{d^2} = \frac{(h^2 + k^2 + l^2) \operatorname{sen}^2 \alpha + 2(hk + kl + hl)(\cos^2 \alpha - \operatorname{cos}^2 \alpha)}{a^2(1 - 3\cos^2 \alpha + 2\cos^3 \alpha)}$$

Ortorrômico:
$$\frac{1}{d^2} = \frac{h^2}{a^2} + \frac{k^2}{b^2} + \frac{l^2}{c^2}$$

Monoclínico:
$$\frac{1}{d^2} = \frac{1}{\operatorname{sen}^2 \beta} \left(\frac{h^2}{a^2} + \frac{k^2 \operatorname{sen}^2 \beta}{b^2} + \frac{l^2}{c^2} - \frac{2hl \cos \beta}{ac} \right)$$

Triclínico:
$$\frac{1}{d^2} = \frac{1}{V^2} (S_{11}h^2 + S_{22}k^2 + S_{33}l^2 + 2S_{12}hk + 2S_{23}kl + 2S_{13}hl)$$

Na equação para cristais triclínicos:

$$S_{11} = b^2 c^2 \operatorname{sen}^2 \alpha,$$

$$S_{22} = a^2 c^2 \operatorname{sen}^2 \beta,$$

$$S_{33} = a^2 b^2 \operatorname{sen}^2 \gamma,$$

$$S_{12} = abc^2 (\cos \alpha \cos \beta - \cos \gamma),$$

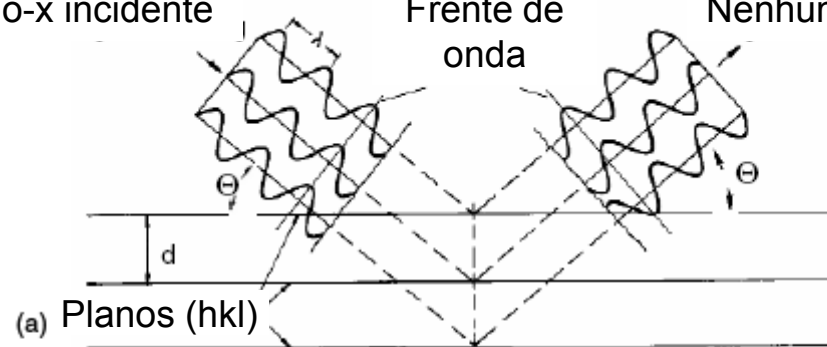
$$S_{23} = a^2 bc (\cos \beta \cos \gamma - \cos \alpha),$$

$$S_{13} = ab^2 c (\cos \gamma \cos \alpha - \cos \beta).$$

Raio-x incidente

Frente de onda

Nenhum raio-x refletido

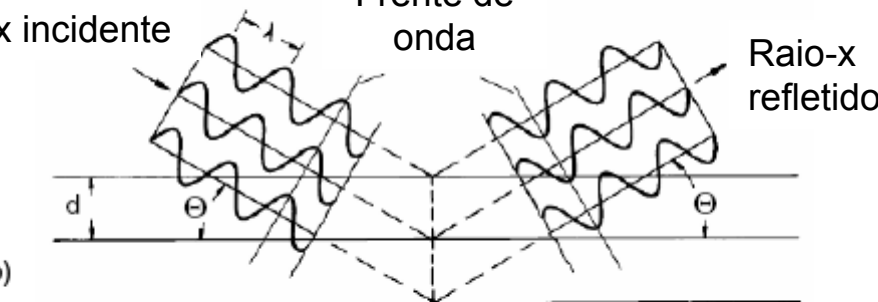


(a) Planos (hkl)

Raio-x incidente

Frente de onda

Raio-x refletido

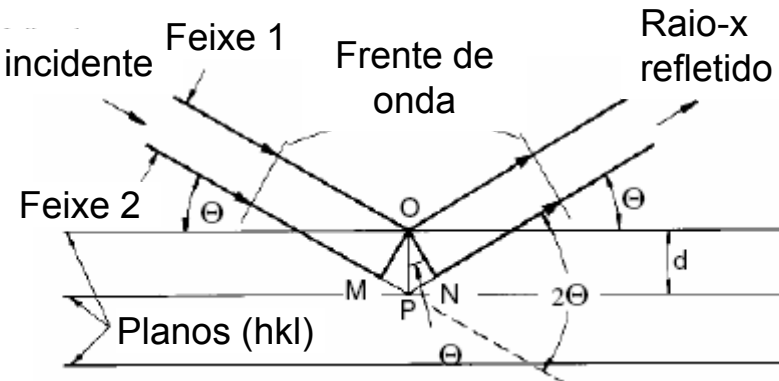


(b)

Raio-x incidente

Frente de onda

Raio-x refletido



(c)

O fundamento teórico do estudo de cristais por raio-X, nêutrons ou elétrons é a Lei de Bragg, a qual descreve a difração de ondas no reticulado cristalino:

$$n\lambda = 2d \sin \Theta$$

aonde λ é o comprimento de onda, d é a distância interplanar, θ é o ângulo de incidência e reflexão e n é a ordem do reflexo.

$$\mathbf{Q} = \mathbf{K} - \mathbf{K}_0$$

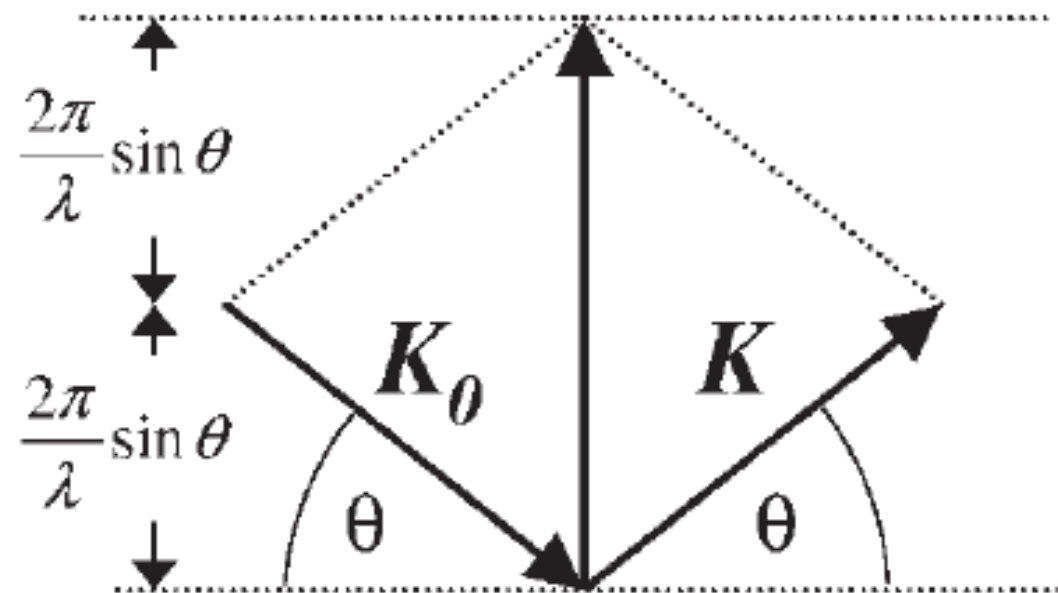


Figure 1.3 Geometry of scattering vector construction.

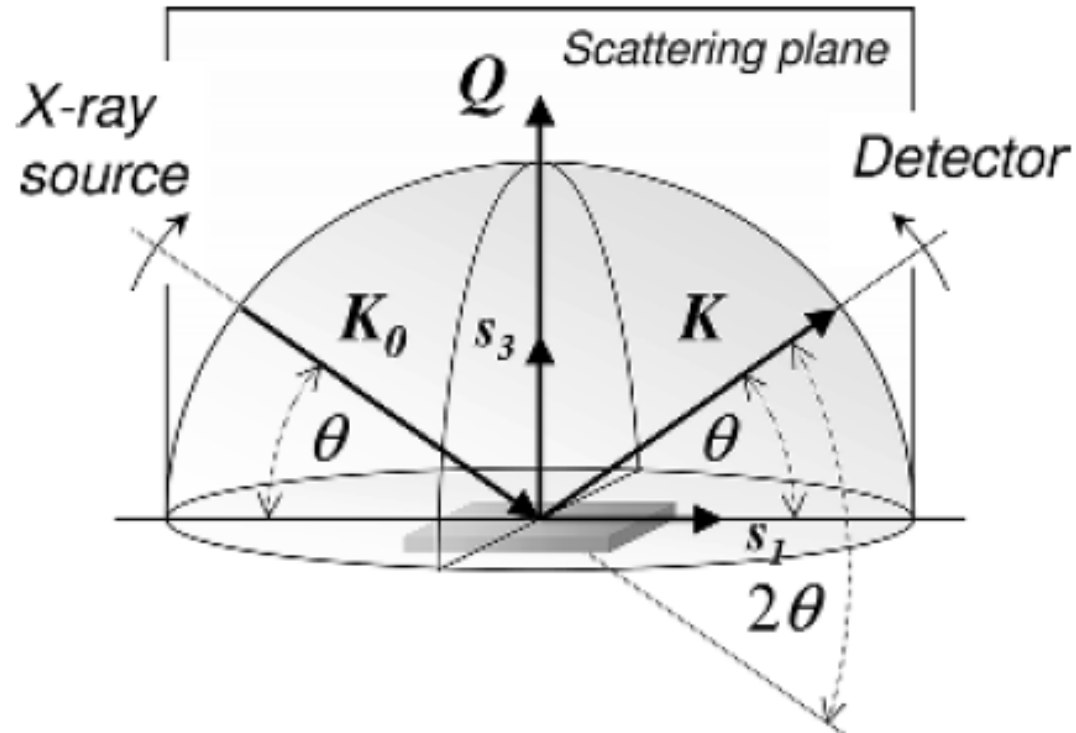
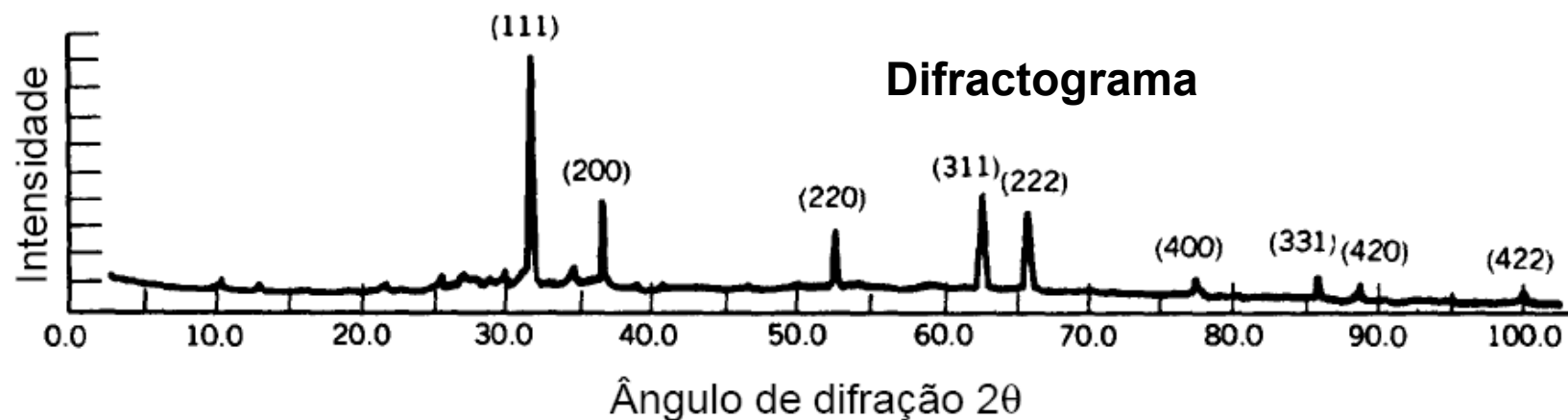
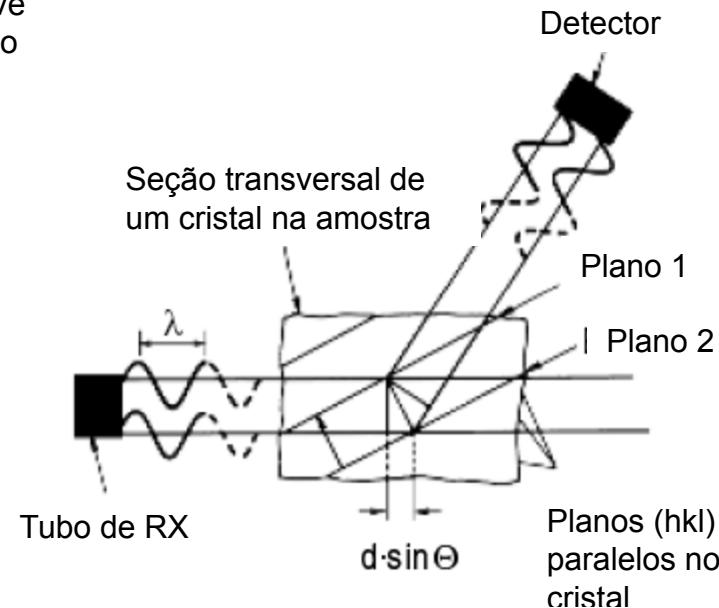
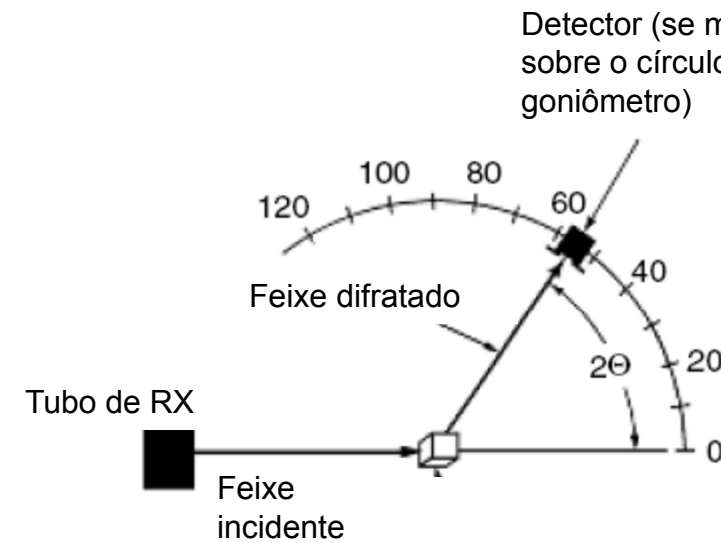


Figure 1.8 Schematic representation of a $\theta/2\theta$ scan from the viewpoint of the sample reference frame $\{s_i\}$.

Difratômetro



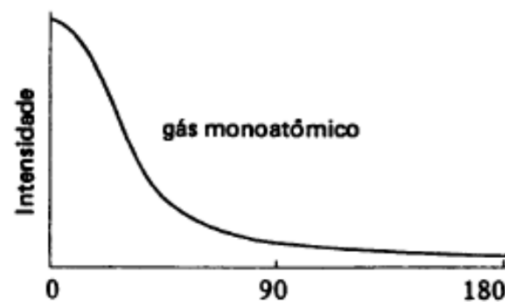
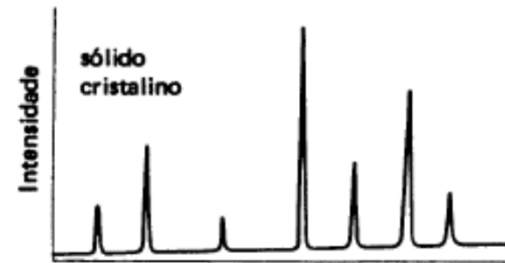
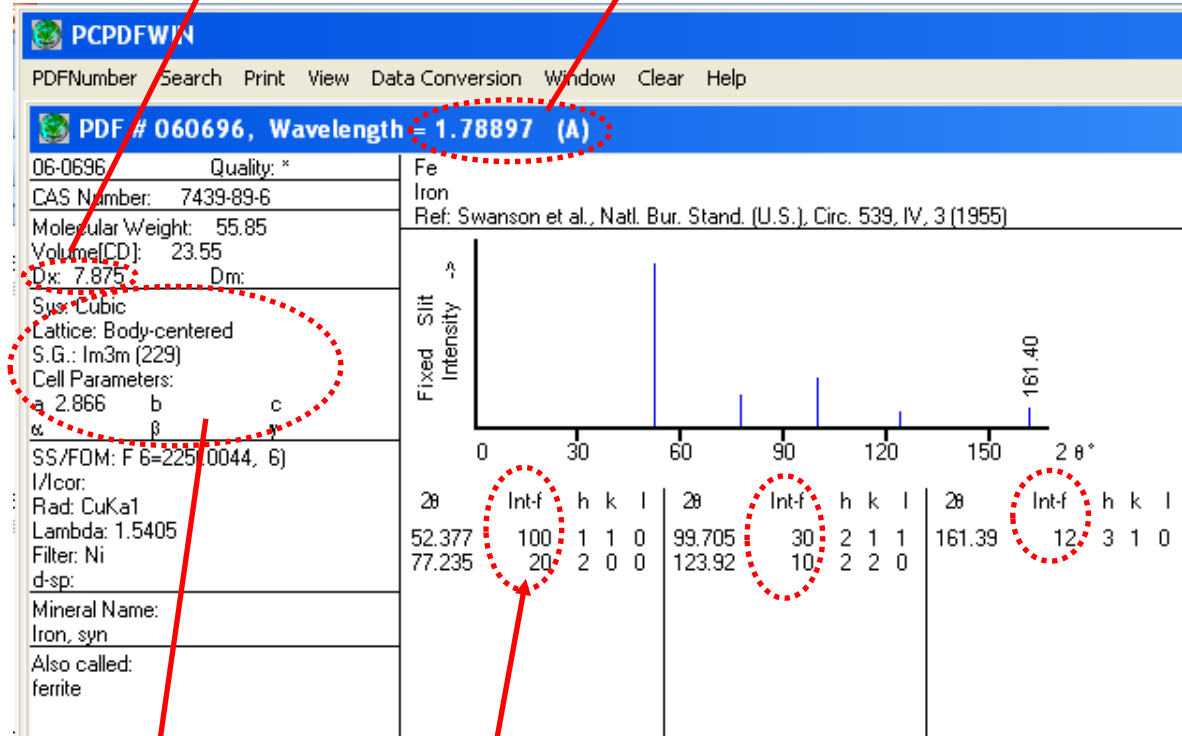


Figura 6.7 — Difratogramas típicos e esquemático de alguns materiais (segundo B.D. Cullity).

Dx = Densidade da fase

Comp. onda λ para cálculo das posições 2θ



Inf. sobre a célula unitária

Pico mais forte da ferrita é o (110) para amostras sem orientação preferencial !! Todas as outras int. teóricas são apresentadas normalizadas com relação ao pico mais forte, o que é normalmente indicado como 100 ou 1000 !!

- Listagens dos picos para as mais diversas fases são encontradas em bancos de dados cristalográficos, como PCPDFWIN, PDF4 e ICSD (esse tem o acesso garantido pela CAPES – Portal da Pesquisa)

- As áreas (intensidades) dos picos de uma fase obedecem razões específicas (intensidades teóricas) no caso dos grãos na amostra possuírem orientação perfeitamente randômica (tipo pó !)

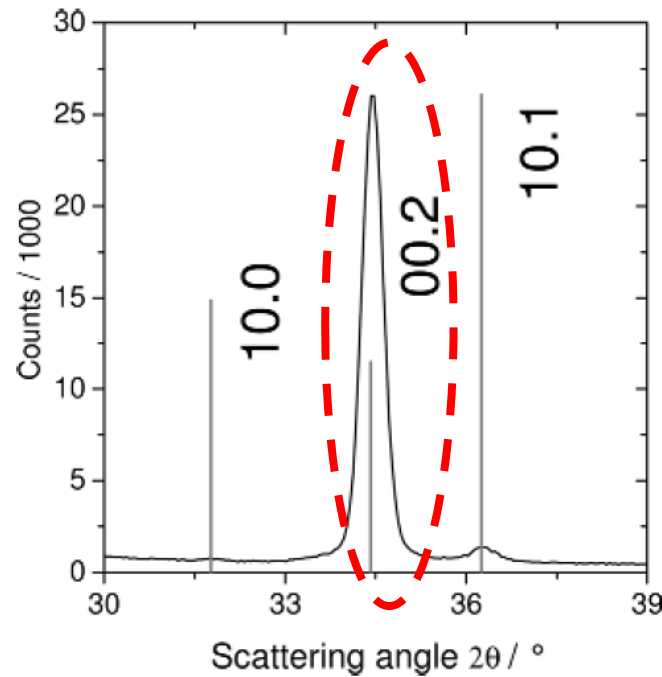
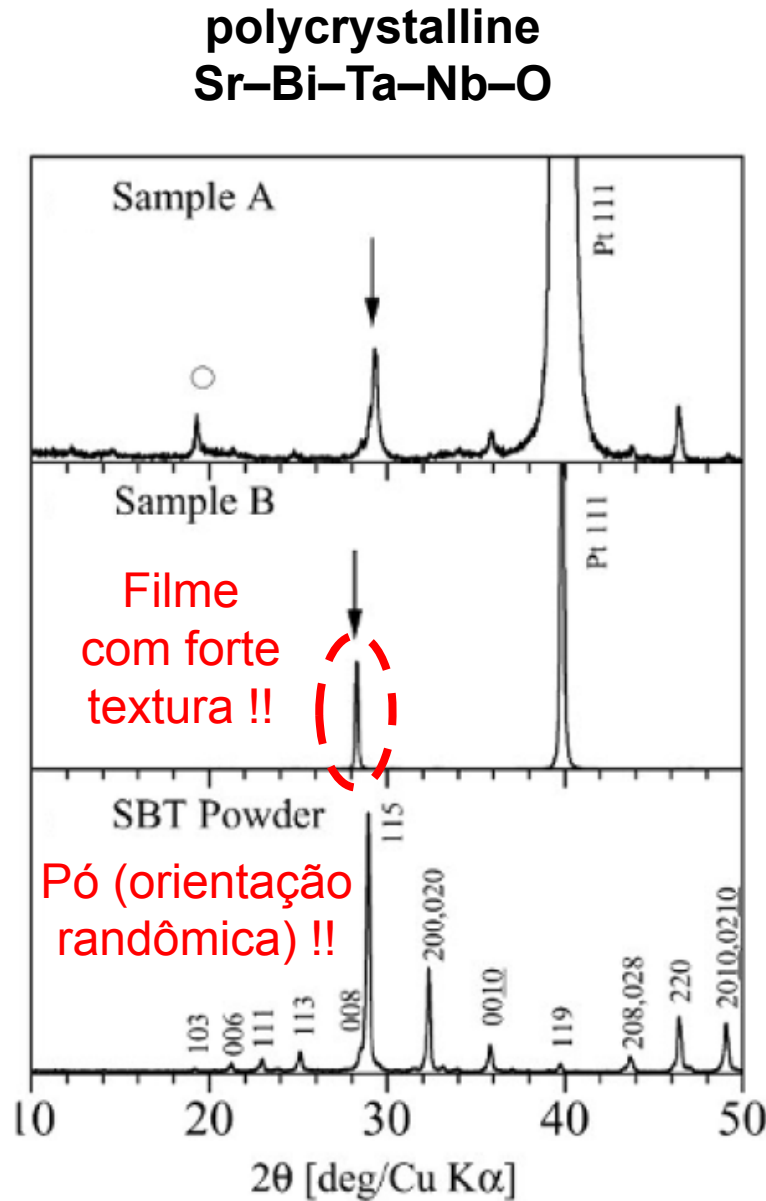
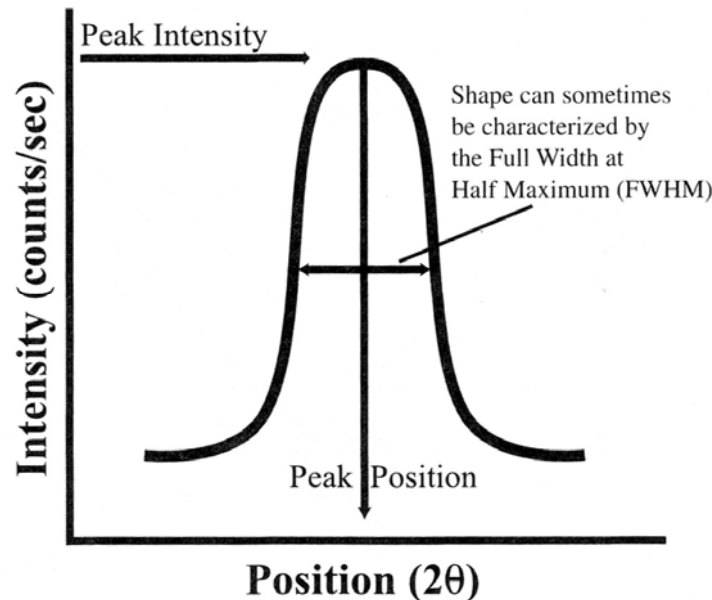


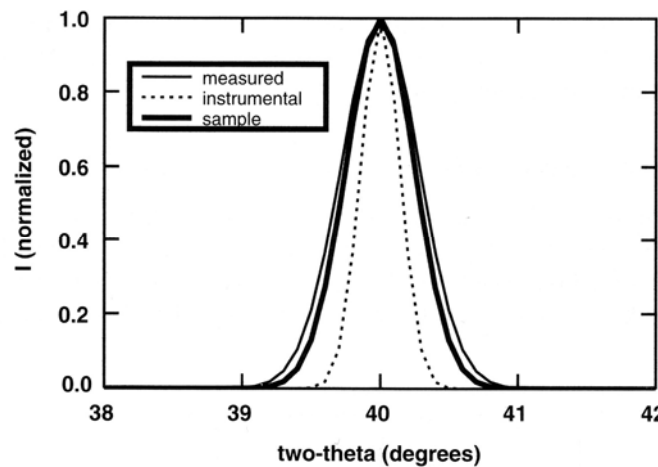
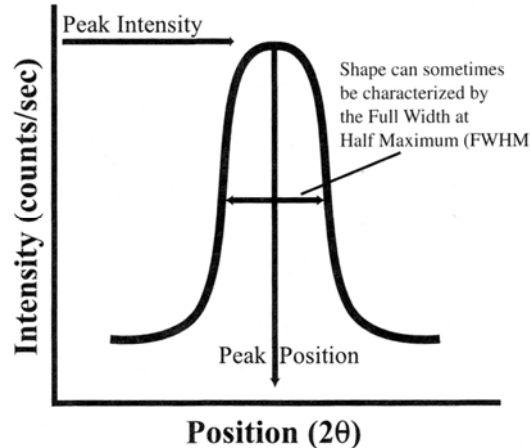
Figure 5.2 Symmetrical $\theta/2\theta$ diffraction pattern of a nominally 500 nm thin ZnO film.

Em geral, ocorre pelo menos um pico muito mais intenso (que o previsto pelas Intensidades teóricas !!) que os demais, que podem até desaparecer completamente !!



Elementary parameters which describe a diffraction peak are:

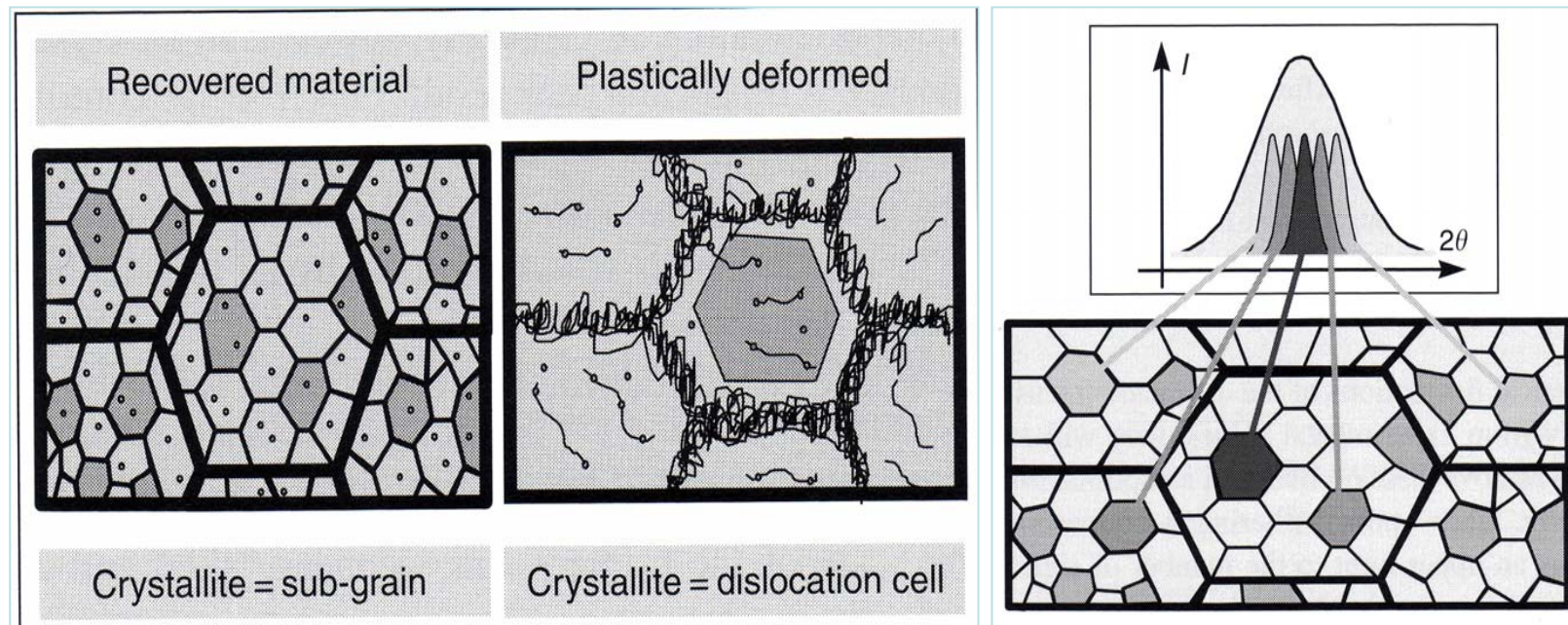
- peak position, depends on temperature, strain, chemical composition of the diffracting domain
- peak intensity, which is related to the volume of the diffracting domain (e.g. phase volume fraction, texture contribution)
- peak shape, which is related to the size of the diffracting domains and the 3rd order microstresses



- $h(2\theta) = [f(2\theta) \otimes g(2\theta)] + bkg$
- The **measured** $h(2\theta)$ profile is a convolution of the **instrument** $g(2\theta)$ and **sample** $f(2\theta)$ profiles
- The instrumental part has to be deconvoluted !!

Microstructural Broadening due to

- *Particle Size D*: Domains D, Stacking Fault Probability α , Twinning Probability β , Chemical Order
- *Microstrains $\langle \varepsilon \rangle$* : Dislocations, Precipitates, Particles



Definition of a crystallite and physical generation of a diffraction peak /Sprauel/

- the shape of the diffraction peak depends on the microstructure of the material studied and gives information about 3rd order RS
- the reflection results from coherently diffracting periodic structures of a crystal named coherently diffracting domains. Discontinuities such as dislocations will not participate, but lead to diffuse scattering.

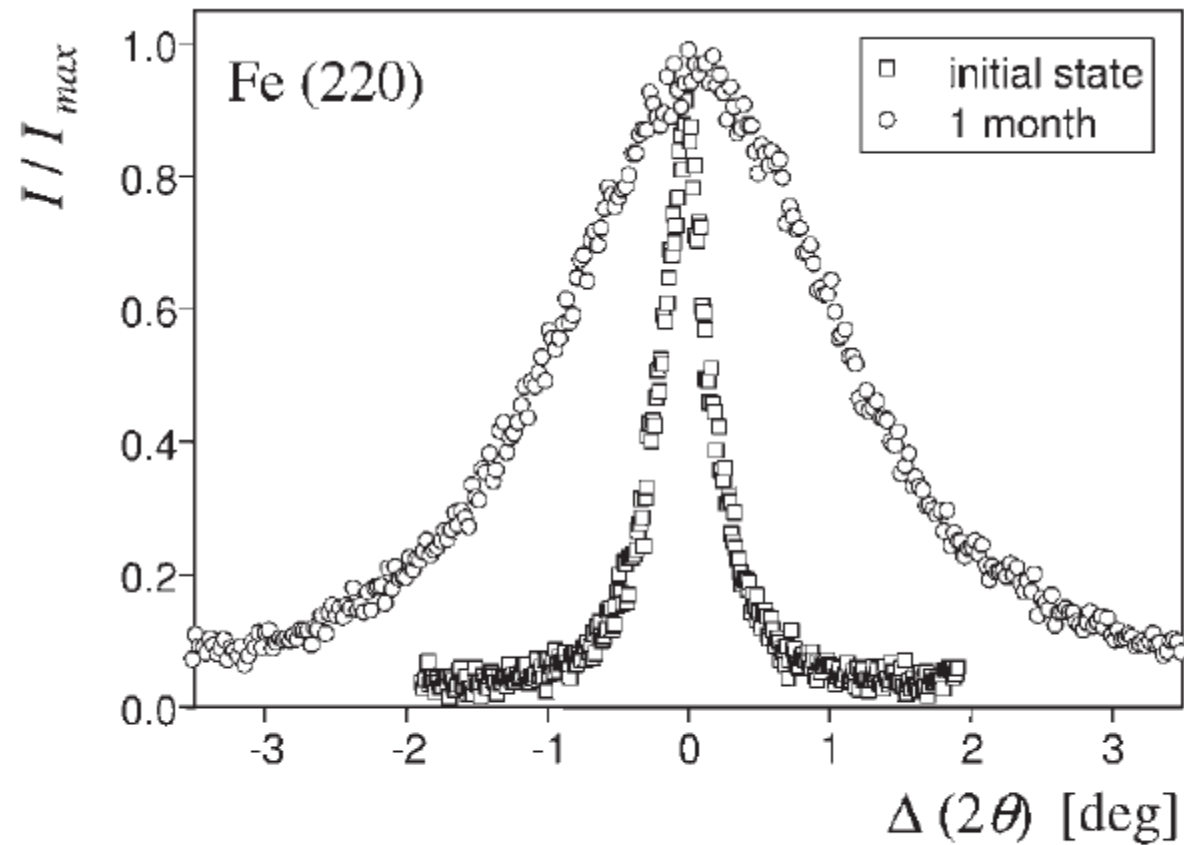


Figure 3.12 Normalized 220 reflections of an unprocessed and ball-milled iron powder (compare to Ref. [31]).

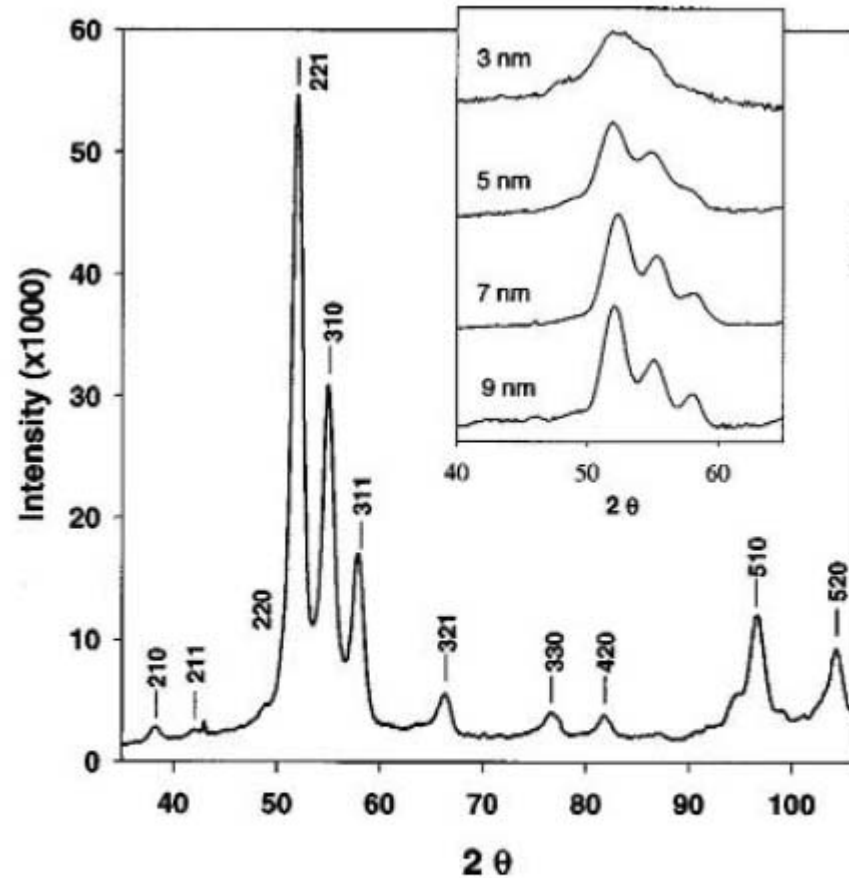
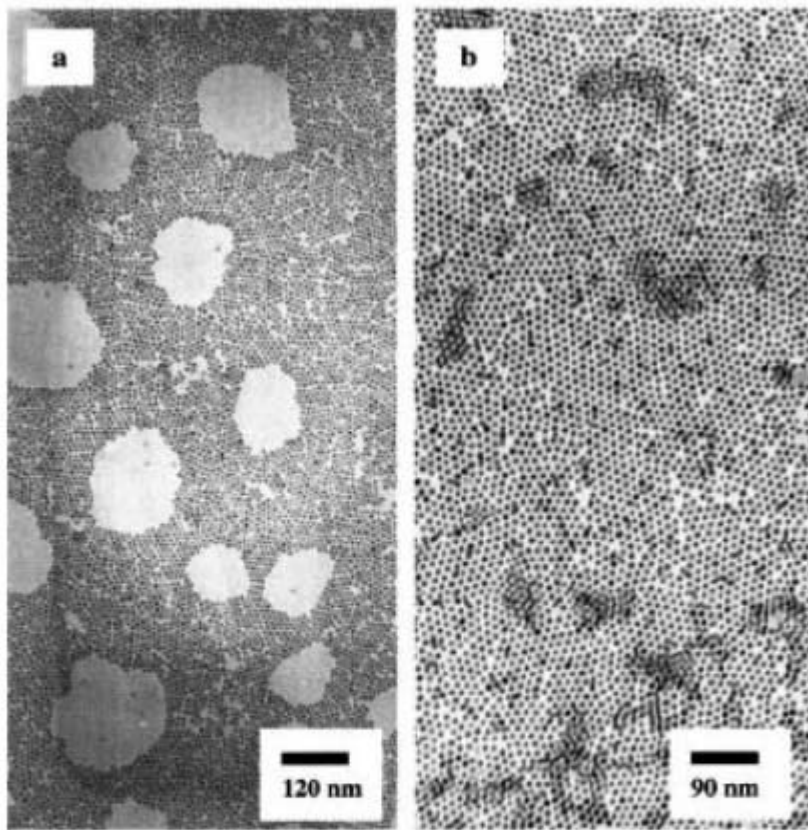
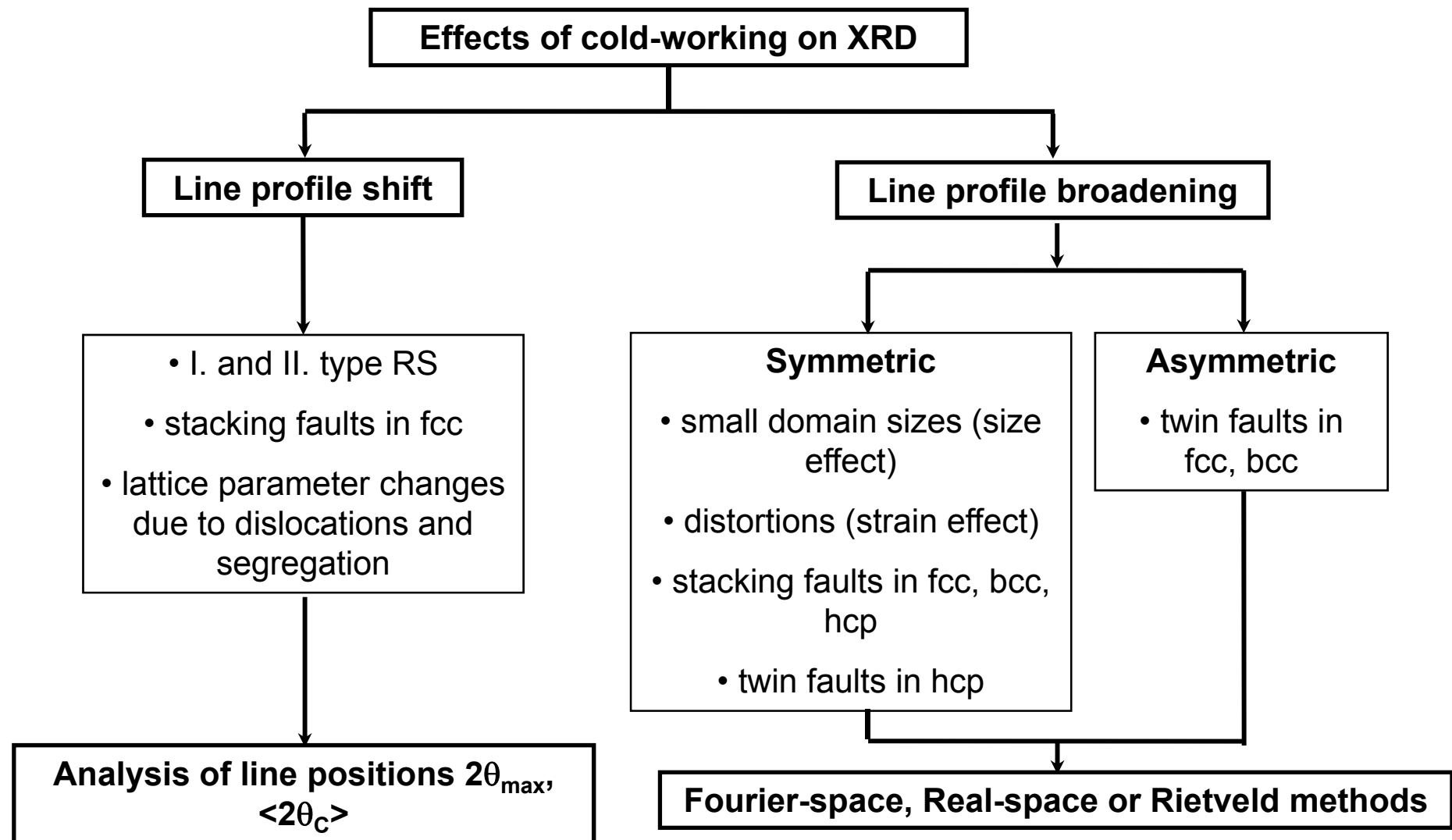
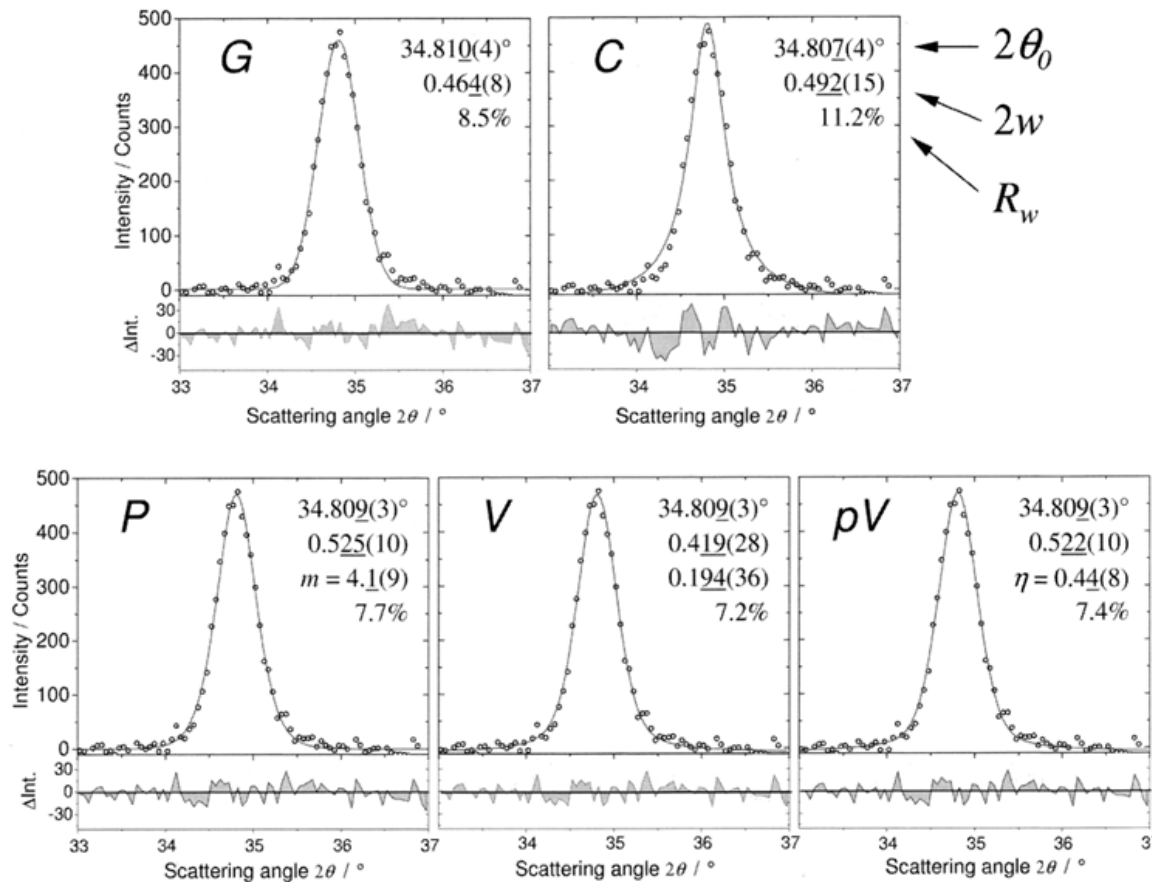


Figure 3.7 TEM images of Co nanoparticles with grain sizes of (a) 6 nm and (b) 9 nm. (c) Symmetric $\theta/2\theta$ diffraction pattern of 11 nm ϵ -phase Co nanocrystals measured with Co

κ radiation. Inset: Large-peak region for nanocrystals of decreasing size (from Ref. [24]).





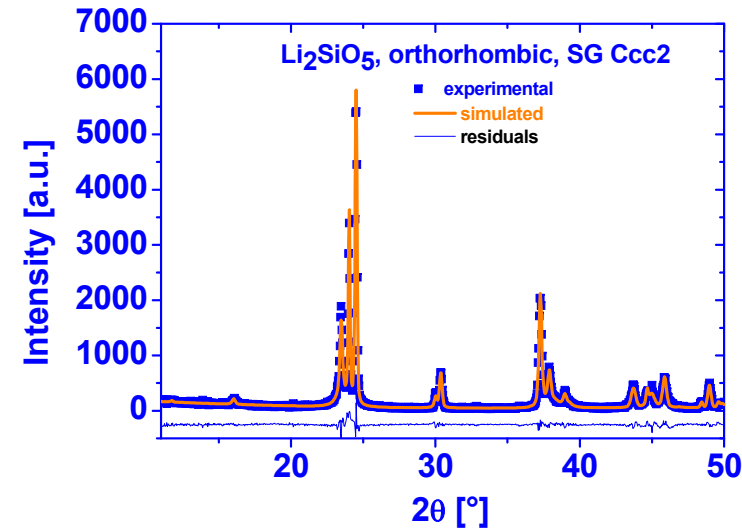
Diffraction lines are described by analytical functions.

$$f_V = \frac{\beta}{\beta_C \beta_G} \int_{-\infty}^{+\infty} f_C(\zeta) f_G(2\theta - \zeta) d\zeta \quad (\text{Voigt}); \quad f_{pV} = \eta f_C(2\theta) + (1 - \eta) f_G(2\theta) \quad (\text{pseudo-Voigt})$$

When the diffraction lines at least partially overlap, as in case of **multi-phase materials or low-symmetry phases**, structure refinement by **Rietveld techniques** is the method of choice.

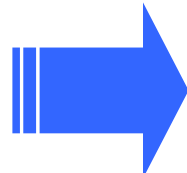
$$I_i^{calc} = Bkg_i + \sum_{n=1}^N S_n \sum_{k=1}^K j_{nk} Lp_{nk} P_{nk} |F_{nk}|^2 \Omega_{ink}$$

S_n scale factor, j_{nk} multiplicity, Lp_{nk} Lorentz-polarisation factor, P_{nk} correction for preferred orientation, $|F_{nk}|^2$ structure factor, Ω_{ink} line profile function, n phases, k reflections



Input

- instrument characteristics
- unit cells, thermal vibrations
 - sample characteristics (absorption, excentricity, etc.)



Output

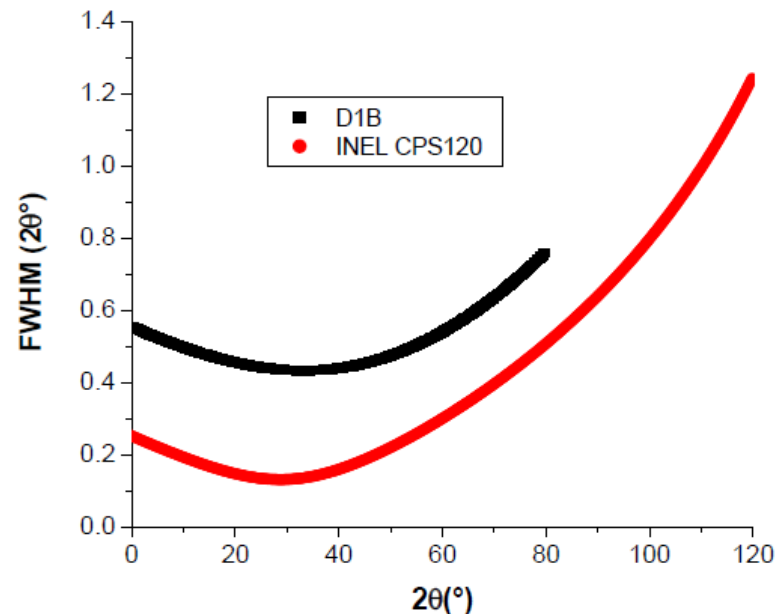
- phase fractions
- crystallite sizes, microstrains
 - SF, twin probabilities
- preferred orientations

It is interesting to note that $g(x)$ is depending on the variable used in the experiment (Bragg angle in constant-wavelength set-up or wavelength for energy dispersive instruments for instance). The angular variation of the full-width at half-maximum H (or FWHM) of the diffraction lines is usually represented by the Cagliotti et al. [1958] relationship:

- 3

$$\text{HWHM}^2 = H^2 = U \tan^2\theta + V \tan\theta + W$$

This form includes the one proposed by Khattak et Cox (1977) as a simplification in the case of X-ray diffraction diagrams. Note here that we should not confuse the FWHM (which is called sometimes "Halfwidth", particularly in pioneering works) and HWHM (Half Width at Half Maximum) the half of the former.



The structure factor is given by [Eberhardt 1976]:

- 28

$$F_{\mathbf{k}} = \sum_j N_j f_j \exp(2\pi[hx_j + ky_j + \ell z_j]) \exp(-M_j)$$

with:

- h, k, ℓ : Miller indices
- x_j, y_j, z_j : atomic positions of the atom j in the unit-cell
- f_j : atomic scattering factor for atom j

The X-ray scattering factor is defined as:

- 29

$$f_j(\sin\theta/\lambda) = f_0 + f' + if''$$

where f_0 is the normal atomic scattering factor, f' and f'' are the real and imaginary dispersion terms respectively which account for the anomalous scattering.

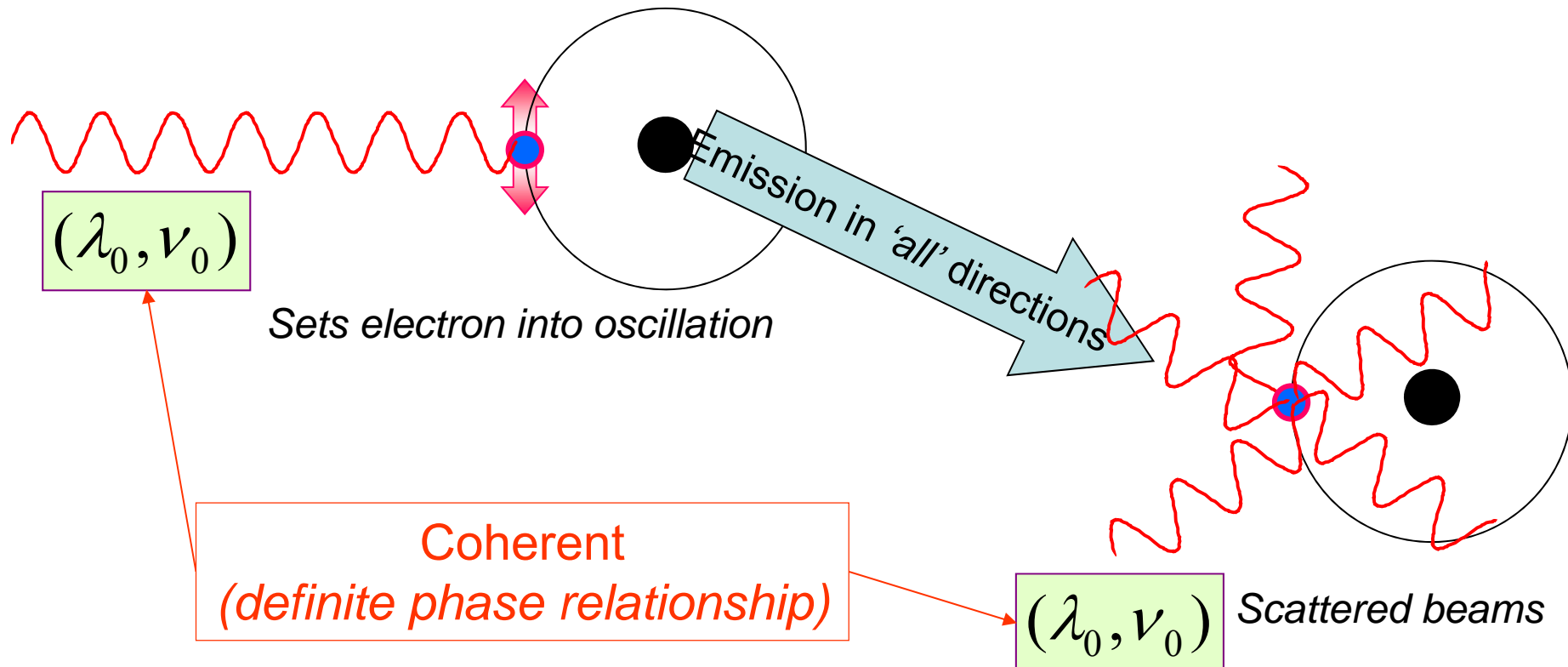
The f_0 values may alternately be calculated using the formula:

- 30

$$f_0(\sin\theta/\lambda) = \sum_{i=1}^4 [a_i \exp(-b_i(\sin\theta/\lambda)^2)] + c$$

The nine coefficients $a_i, b_i, i = 1$ to 4 and c can be retrieved by the programs simply by supplying the atom name (neutral atoms and ions, e.g. Sr^{2+} , O^{2-} etc.).

- N_j : occupation ratio of site j
- $\exp(-M_j)$: thermal vibration parameter



- The electric field (**E**) is the main cause for the acceleration of the electron
- The moving particle radiates most strongly in a direction perpendicular to its motion
- The radiation will be polarized along the direction of its motion

Scattering by an atom \propto [Atomic number, (path difference suffered by scattering from each e^- , λ)]

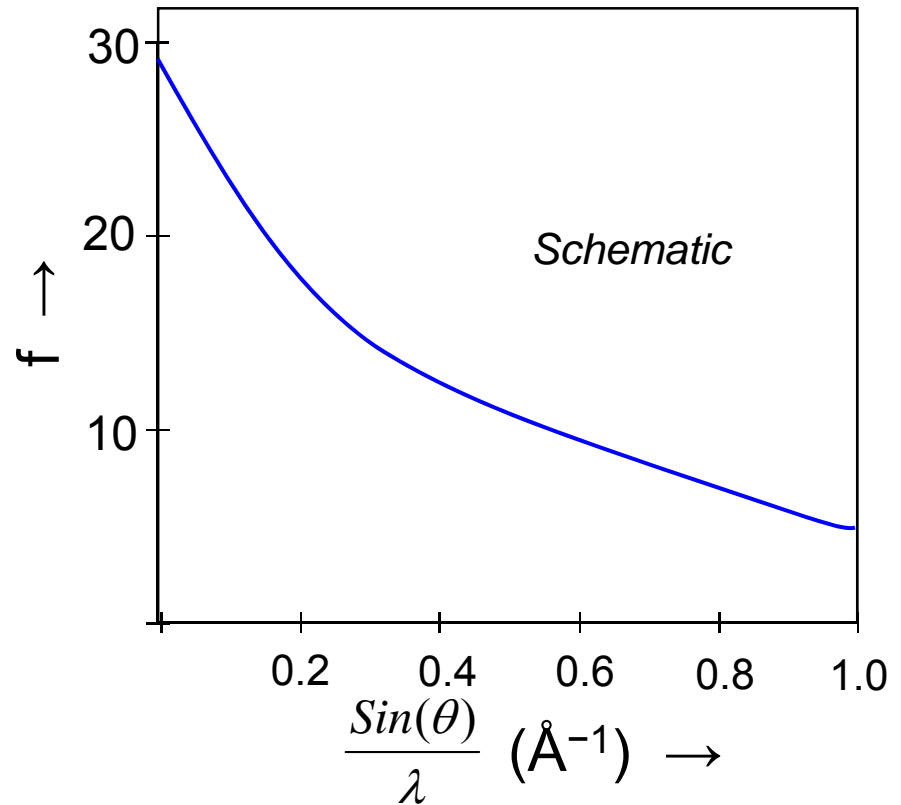
Scattering by an atom \propto $[Z, (\theta, \lambda)]$

$$\frac{\sin(\theta)}{\lambda}$$

- Angle of scattering leads to path differences
- In the forward direction all scattered waves are in phase

f = Atomic Scattering Factor

$$= \frac{\text{Amplitude of wave scattered by an atom}}{\text{Amplitude of wave scattered by an electron}}$$



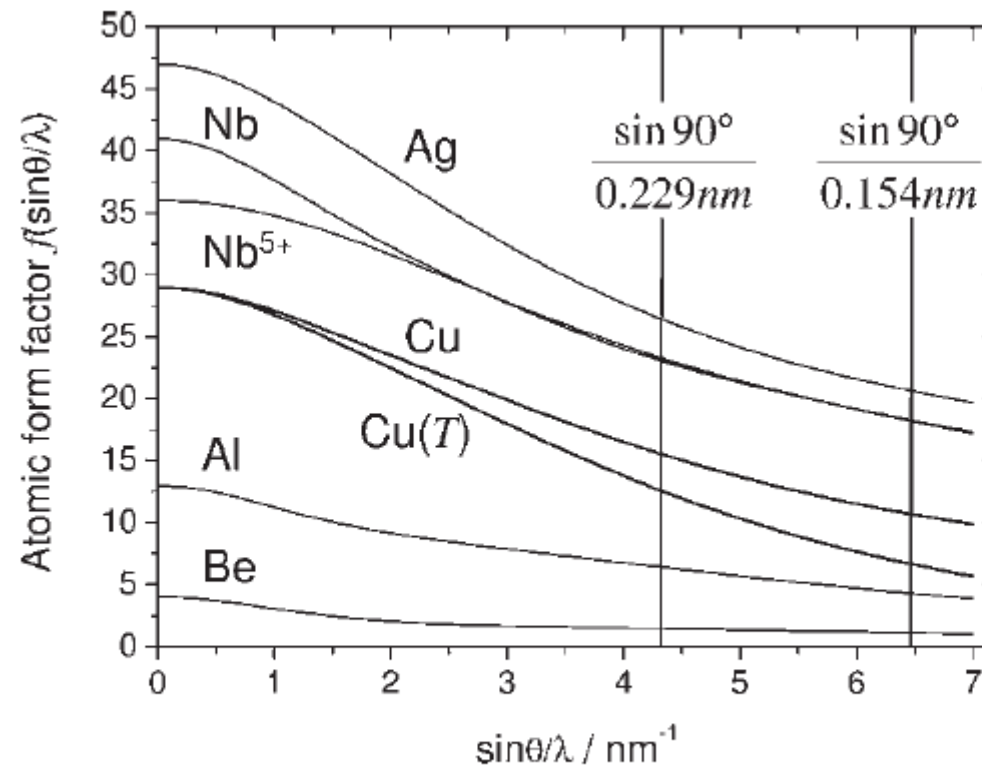


Figure 1.11 Atomic form factors of Be, Al, Cu, Cu@fccCuRT, Nb, Nb^{5+} and Ag.

Regarding the effect of thermal vibrations the same arguments apply as given above to justify the reduction in coherency by the spatial extension of electronic charge distribution. It is well known that the atoms in a solid oscillate at their equilibrium positions \mathbf{r}_n . Temperature vibrations entail a reduction of phase coherence in the scattered beam and thus reduce the measured intensity. The phenomenon can quantitatively be accounted for by the mean quadratic deviation u^2 of the atom from its average position r_n . The atomic form factors f have then to be replaced by the temperature-dependent expression

$$f_T = f \exp\left(-8\pi\overline{u^2} \sin^2 \theta / \lambda^2\right) \quad (1.26)$$

Again, it can be seen that the scattering amplitude is exponentially damped with increasing scattering angle and that the damping coefficient scales with the square of momentum transfer $4\pi\sin\theta/\lambda$. The $8\pi\overline{u^2}$ factor is often abbreviated by the symbol B in the literature. Typically the average displacements of atoms $\sqrt{\overline{u^2}}$ at room temperature are in the range between 0.005 and 0.03 nm, which translates into a few percent to more than 10% of the bond length. In the fcc structured Cu lattice, for instance, $\sqrt{\overline{u^2}}$ amounts to about 6% of $d_{\text{Cu-Cu}}$. The effect of the temperature vibrations can be seen from Fig. 1.11, where in addition to the zero-temperature f also the atomic form factor of Cu in the Cu lattice is shown. It is evident that the scattering strength may be significantly reduced by thermal vibration, which holds in particular for high scattering angles.

These results are applied to the structure factor simply by replacing the form factor with its temperature-dependent value

$$F_{hkl}(T) = \sum_{n=1}^N f_n \exp\left(-B_n(T)\sin^2\theta / \lambda^2\right) \exp\left(2\pi i(hx_n + ky_n + lz_n)\right) \quad (1.27)$$

Because the thermal vibration amplitudes increase with increasing temperature the damping of Bragg reflections will also increase. This causes the Bragg reflection to sink into a background of diffuse scattered intensity when the temperature is increased. This is in contrast to many spectroscopic techniques, where the observed peaks broaden at elevated temperature.

Here are the atomic parameters which may be specified:

- 1) The Atomic Scattering Factor which may include both nuclear and magnetic scattering for neutron diffraction, or real and anomalous scattering for X-ray diffraction.
- 2) The Site Occupation Factor, which may reflect genuine defects in the occupancy of a particular atomic site, or, more usually, is employed to produce correct structure factor contributions from atoms situated on crystallographic symmetry elements.
- 3) The Coordinates within the unit cell expressed relative to the possibly non-orthogonal unit cell axes in terms of fractions of the unit cell edge.
- 4) The Thermal vibration parameters, which may describe either isotropic or anisotropic vibration. The isotropic temperature correction to the calculated structure factor is:
5)

- 31
$$\exp[-B(\sin \theta / \lambda)^2]$$

where B is the temperature factor expressed in \AA^2 . It then is the mean quadratic displacement of the atom. The anisotropic correction for reflection (hkl) is:

- 32
$$\exp - [h^2 \beta_{11} + h^2 \beta_{22} + \ell^2 \beta_{33} + 2hk\beta_{12} + 2h\ell\beta_{13} + 2k\ell\beta_{23}]$$

where β_{11} to β_{23} are the unique elements of the symmetric tensor describing the thermal vibration ellipsoid.

Table s1.1 The three most common crystal structures of one-elemental metals. Unit cell edges under standard conditions are given.

Structure	Strukturbericht designation	Space group	Atomic positions		Examples with lattice parameters a and c (nm)
Face-centered cubic (fcc)	Copper structure (A1)	$Fm\bar{3}m$ (225)	000	$0\frac{1}{2}\frac{1}{2}$	Al: 0.4049; Ni: 0.3524
Body-centered cubic (bcc)	Tungsten structure (A2)	$I\bar{m}\bar{3}m$ (229)	$\frac{1}{2}0\frac{1}{2}$	$\frac{1}{2}\frac{1}{2}0$	Cu: 0.3615; Ag: 0.4086
Hexagonal close-packed (hcp)	Magnesium structure (A3)	$P6_3/mmc$ (194)	000	$\frac{2}{3}\frac{1}{3}\frac{1}{2}$	Cr: 0.2884; Fe: 0.2866 Nb: 0.3307; W: 0.3165

The majority of one-elemental metals are found in either the face-centered cubic (fcc), the body-centered cubic (bcc) or the hexagonal close-packed (hcp) structure. The relative arrangement of atoms in these lattices is presented in Structure Box 1. Aluminum, for instance, crystallizes in the fcc structure. In this case the Bragg equation might be obeyed for certain lattice planes hkl , but for some combinations of hkl the phase shift in the x-rays scattered by neighboring atoms may amount to π or odd multiples of it. The scattered beams then interfere destructively and the reflections for these lattice planes are not extinguished. In the fcc structure, for instance, destructive interference occurs for $hkl = 100, 110$, etc.

The extinction conditions can be derived for any crystal lattice by performing the same summation procedure that has been performed for the simple cubic lattice in the first section and it is an instructive exercise to do so (Exercise 7). One will then arrive at conditions comparable to Eq. (1.11) which predict under which orientation of \mathbf{Q} towards $\{\mathbf{s}_i\}$ reflections might be observed. A simpler approach instead is the calculation of the structure factor. Inserting the fractional coordinates of all four atoms of the fcc structure in Eq. (1.23) yields the result

$$F_{\text{fcc}}(hkl) = f \left[1 + \exp(i\pi(h+k)) + \exp(i\pi(h+l)) + \exp(i\pi(k+l)) \right] = \begin{cases} 4f & \text{all } hkl \text{ even/odd} \\ 0 & hkl \text{ mixed} \end{cases} \quad (1.24)$$

The expression is seen to vanish for certain hkl and the lower equation is thus denoted as an extinction condition. It means that Bragg reflections are only observed for the fcc lattice if all Miller indices are either even or odd. For mixed triples destructive interference occurs and these reflections are systematically absent. It is evident from the $\theta/2\theta$ scan in Fig. 1.10 that this pattern in fact is in accordance with the extinction conditions of the fcc structure. Mathematically speaking, the Bragg equation is a necessary but not a sufficient condition for x-ray reflections to arise.

The structure factor of the bcc lattice can be obtained in the same way and results in

$$F_{\text{bcc}}(hkl) = f \left[1 + \exp(i\pi(h+k+l)) \right] = \begin{cases} 2f & h+k+l = 2n \\ 0 & \text{otherwise} \end{cases} \quad (1.25)$$

The extinction condition now derives from a sum over Miller indices and reads that the sum must yield an even number for the reflection to occur. Only if this condition is obeyed is the interference nondestructive and can be detected at the position predicted by Bragg's equation (Eq. (1.15)). The structure factor for the hcp structure can be derived as an exercise from the atom coordinates in the unit cell.

The structure factor F_h from a reflection h is of central importance in x-ray diffraction, because it relates the position of the atoms in the unit cell to the intensity of a reflection. Here, the Miller index triple hkl has been abbreviated by the sub-

$\{h k l\}$	kubisch	tetragonal	hexagonal	orthorhombisch	monoklin	triklin
$\{h k l\}$	48	16	24	8	4	2
$\{h h l\}$	24	8	12	8	4	2
$\{h l h\}$	24	16	24	8	4	2
$\{l h h\}$	24	16	24	8	4	2
$\{h k 0\}$	24	8	12	4	2	2
$\{h 0 l\}$	24	16	12	4	4	2
$\{0 k l\}$	24	16	12	4	4	2
$\{h h h\}$	8	8	12	8	4	2
$\{h h 0\}$	12	4	6	4	2	2
$\{h 0 h\}$	12	8	12	4	4	2
$\{0 h h\}$	12	8	12	4	4	2
$\{h 0 0\}$	6	4	6	2	2	2
$\{0 k 0\}$	6	4	6	2	2	2
$\{0 0 l\}$	6	2	2	2	2	2

The correction of preferred orientations has to be taken into account as soon as the crystallites are likely to orient in one or several directions of the sample. Texture is particularly present in easy-clivage materials or having anisotropic growing, and when the samples are elaborated by anisotropic techniques. For instance NaCl crystallises as parallelepipedic crystallites limited by (001) planes which tend to orient parallel to the sample surface when compacting it for measurement purposes. In Bragg-Brentano geometry, the corresponding intensities will be favoured.

One should not confuse the texture effect and the lack in statistics in terms of number of irradiated crystallites, which both reinforce some peaks. In the latter case, reinforcements appear more or less stochastically, while in the former all the hkl , $2h2k2l$, $3h3k3l$, ..., are reinforced (if hkl is the textured direction).

It exists two types of texture treatments in Rietveld analysis. If the texture is simple (high symmetry and regular dispersion), it can be modelled by a classical analytical shape (Gaussian ...). If it is more complex (several texture components, non regular distributions ...) the treatment requires a quantitative texture analysis, matter of §5. In this paragraph only the simplest textures are of concerns.

The texture can be roughly modelled using three parameters:

- a texturation axis linked to the sample symmetry (the normal to the sample surface for a flat sample in Bragg-Brentano geometry, the cylinder axis in Debye-Scherrer geometry)
- the crystallographic direction h which tends to align with the previous axis
- a texturation strength (angular dispersion, texturation factor ...).

2.3.3.2 March–Dollase approach

Dollase shown that the following function is more efficient [Dollase 1986, Bowman et Mendendorp 1994]:

- 35

$$P_h = \left(G_1^2 \cos^2 \alpha_h + \left(\frac{1}{G_1} \right) \sin^2 \alpha_h \right)^{-\frac{3}{2}}$$

where α is the acute angle between the scattering vector and the preferred orientation axis. Originally, the correction assumed a Gaussian distribution of the preferred orientation axis of the individual crystallites about the normal to the plane of the sample. G_1 is the refinable parameter ($G_1 = 1$: no preferred orientation) that now controls the distribution shape and is an index of the preferred orientation strength ($G_1 = 1$ for a random orientation).

This model provides:

- a preferred orientation correction factor which minimum or maximum at $\alpha = 0^\circ$
- a symmetric and smooth evolution in the $[0, 90^\circ]$ α range
- a single parameter to be fitted
- the possibility of normalisation of the orientation:

- 36

$$\int_0^{\frac{\pi}{2}} P_h d\alpha = 1$$

This latter property is important in order to keep constant the total diffracted intensity in a diffraction diagram whatever the distribution shape P_h .